[5]Thompson, P. M., Myers, T. T., and Suchomel, C., "Conventional Autopilot Design for a Hypersonic Vehicle," AIAA Paper 95-0556, Jan. 1995.

[6]Larson, G. L., Klyde, D. H., Myers, T. T., and McRuer, D. T., "Military Missions and Linearized Model for a Hypersonic Vehicle," AIAA Paper 95-0851, Jan. 1995.

[7]Vu, P. T., and Biezad, D. J., "Direct-Lift Design Strategy for Longitudinal Control of Hypersonic Aircraft," *Journal of Guidance, Control, and Dynamics*, Vol. 17, No. 6, 1994, pp. 1260–1266.

[8]Schmidt, D. K., and Velapoldi, J., "Optimum Mission Performance and Guidance for Hypersonic Single Stage to Orbit," AIAA Paper 96-3904, July 1996.

[9]Schmidt, D. K., "Optimum Mission Performance and Multivariable Flight Guidance for Airbreathing Launch Vehicles," *Journal of Guidance, Control, and Dynamics*, Vol. 20, No. 6, 1997, pp. 1157–1164.

[10]Sachs, G., Schoder, W., and Kraus, W., "Separation of Lifting Vehicles at Hypersonic Speed—Wind Tunnel Tests and Flight Dynamics Simulation," *Space Systems Design and Development Testing*, AGARD CP 561, 1995, pp. 5-1–5-8.

[11]Bowers, A., Noffz, G., Gonda, M., and Iliff, K., "A Generic Hypersonic Aerodynamic Model Example (GHAME)," NASA Dryden Flight Research Center, Edwards AFB, CA, 1989.

[12]Meyer, I., McMaster, I., and Moody, R., "Handling Qualities of the SR-71," Lockheed Aircraft Corp., Rept. SP-508, Advanced Development Projects, Burbank, CA, Sept. 1978.

[13]Heffley, R., and Jewell, W., "Aircraft Handling Qualities Data," NASA CR 2144, Dec. 1972.

[14]Sachs, G., "Path-Attitude Decoupling and Flying Qualities Implications in Hypersonic Flight," *Aerospace Science and Technology*, Vol. 2, No. 1, 1998, pp. 49–59.

Design Methods for Rocket Attitude Control Systems Subject to Actuator Saturation

Hyung Don Choi,* Hyochoong Bang,† and Zeen Chul Kim‡
Korea Aerospace Research Institute, Daejon 305-600, Republic of Korea

Introduction

THE KSR Korea sounding rocket (KSR-II) is a two-stage sounding rocket with a payload capacity of about 150 kg. It is launched near vertically up to the altitudes in the 150-km range to carry out upper atmospheric experiments including ozone layer, ionospheric, and celestial x-ray measurement. A guidance and control (G&C) system is onboard to minimize the dispersion radius of the impact point. This system keeps the flight experiments less sensitive to meteorological conditions, wind in particular, by reducing the impact dispersion considerably. The attitude and angular velocities of the rocket necessary for the construction of the G&C system are obtained from an inertial navigation system (INS). Furthermore, a pneumatic S-19 (Ref. 1) actuator is adopted as a primary actuator system. The actuator saturation of the S-19 is a main element, which may degrade the performance of the whole system. For a controller with an integrator, the saturation effect is accumulated in the integrator, which increases the overshoot resulting in a high settling time.[2] This phenomenon is known as windup[2–5] and usually results in performance degradation.

Received April 13, 1998; revision received Aug. 19, 1998; accepted for publication Aug. 20, 1998.

*Senior Research Scientist, Sounding Rocket Group, P.O. Box 113, Yusung-Gu.

†Research Scientist, Koreasat Group, P.O. Box 113, Yusung-Gu. Member AIAA.

‡Senior Research Scientist, Head of Satellite Bus Department, P.O. Box 113, Yusung-Gu.

The primary goal of this Note is to apply the antiwindup controller (AWC) to KSR-II attitude control. There have been extensive studies with well-developed theories on AWC, including stability analysis.[2–5] A rather simple form of AWC, however, is applied to the practical problem of launch vehicle control in this study. The control design is viewed from application perspectives instead of conducting theoretical development. A modified AWC also is introduced, which compensates the highly gain-sensitive characteristics of the typical AWC.

Description of KSR-II Control System

The control system of the KSR-II consists of an INS, a controller, the S-19, and rocket aerodynamics. Because the shape of the KSR-II is long and slender, the magnitude of the roll moment of inertia is approximately 1/100 of the pitch and yaw moments. The roll angular velocity caused by thrust and fin misalignment is much greater than the pitch and yaw angular counterparts. Thus, an INS with a roll-isolated inertial measurement unit by a gimbal is selected. The INS calculates the pitch and yaw angle by a strap-down technique and measures the roll angle. The KSR-II controls attitude by producing aerodynamic control moments using canard fins actuated by a pneumatic system. This S-19 pneumatic system is designed to accept control inputs in the form of roll-resolved pitch and yaw commands to two pneumatic servos. There are four canards connected in pairs with one pair controlling each lateral axis. S-19 has maximum actuating limits at 22 deg in deflection and 140 deg/s in slew rate. This actuator saturation affects the control system performance and stability significantly. The attitude of KSR-II is controlled by canard fins up to 20 s after launch, corresponding to the thrusting phase of the first and second stages. At the end of the control time, the altitude reaches 9.2 km and the Mach number is 3.0. The maximum value of the rocket natural frequency is about 2 Hz, and the damping coefficient is about 0.06 during the first stage burning and 0.002–0.04 for the second stage. The maximum axial accelerations are 12 and 9 g for the first and second stages, respectively. The dynamic pressure reaches a maximum value at about 22 s after launch.

AWC

To maintain the initial rocket attitude at liftoff for a certain period of time, the following proportional, integral, plus derivative (PID) compensator is designed as

$$\delta_p = k\left(e_p + \frac{1}{T_i}\int e_p\,\mathrm{d}t + T_d\dot{e}_p\right) \tag{1}$$

where $e_p = \theta_c - \theta$ is pitch error, θ_c is pitch command, θ is actual pitch angle, k is controller gain, T_i and T_d are integral and derivative time constants, and δ_p is the compensator output. In this study, $k = 10$, $T_i = 3$ s, and $T_d = 0.3$ s are used, which result in gain margins of 10 and 7.6 dB, phase margins of 43.2 and 34.2 deg, and bandwidths of 28 and 43 rad/s for the first and second stage controls, respectively. For a controller with an integrator, the effect of the actuator saturation is accumulated in the integrator, and the integrator value becomes excessively large, i.e., windup. A partial solution for the windup problem of the KSR-II is sought by applying a typical AWC design technique. Because the limit of deflection angle is more severe than that of slew rate in the S-19, only the actuating limit of deflection angle is considered. The concept of AWC is to reduce the difference between the compensator output and the actuator control input by feeding back the difference caused by the actuator limit. The feedback signals of the difference, as well as the PID compensator, are combined together in the AWC as

$$\delta_p^w = k\left(e_p + \frac{1}{T_i}\int e_p\,\mathrm{d}t + T_d\dot{e}_p\right) - \int f\,\mathrm{d}t \tag{2}$$

where the new error term is defined as

$$f = (k/T_t)\left(\delta_p^w - u_p^w\right) \tag{3}$$

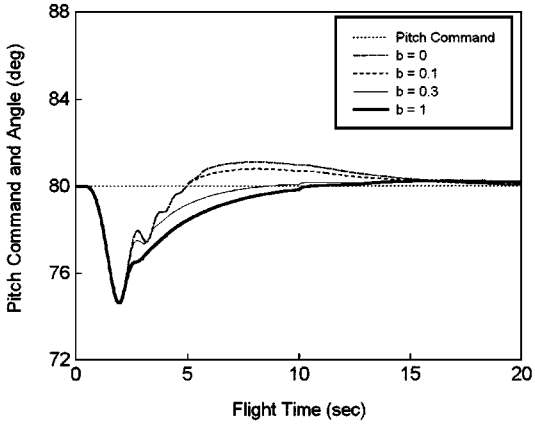

Fig. 1 Effect of AW gain changes on pitch response.

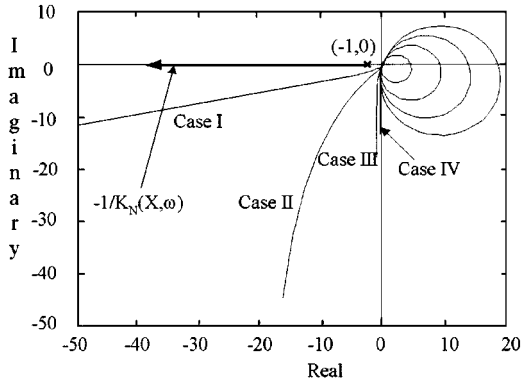

Fig. 2 Nyquist diagram of $G_{eq}(jw)$ using different numbers in b.

and

$$u_p^w = \begin{cases} \delta_p^w : -22 < \delta_p^w < 22 \\ 22 : \delta_p^w > 22 \\ -22 : \delta_p^w < -22 \end{cases} \tag{4}$$

where δ_p^w (degrees) is the compensator output in AWC, u_p^w (degrees) is the actuator control input, f is the antiwindup (AW) feedback signal, and T_t is the AW tracking time constant. If the actuator reaches a saturation limit, the AWC works in the direction to reduce the compensator output by integrating and feeding back the saturated variables. The AW tracking time constant T_t determines the weighting effect of the AW. The ratio of the integrating time constant T_i to T_t is expressed as the AW gain

$$b = T_i/T_t \tag{5}$$

The higher values of this AW gain tend to bring a larger AW effect. Figure 1 compares the simulation results of the rocket attitude changes for the PID (in the case of $b = 0$) and the AW controller. Wind speed of 12 m/s, the maximum allowed value for launching at the direction of 250 deg (west–south–west), is incorporated into the six-degrees-of-freedom nonlinear simulation. Note that the rocket is launched at the elevation angle of 80 deg and an azimuth of 191 deg, respectively. It undergoes stage separation at 10 s and ignition of the second stage at 12 s controlled until 20 s, after which the canard fins are released to follow the freestream. In case of the PID controller, the error caused by the actuator limit is accumulated in the integrator. When AWC is applied to this particular problem, the performance is improved remarkably. The controller feeds back the difference between the compensator output and the actuator control input to operate the actuator as much in the linear range as possible, reducing the overshoot level. As the AW gain b increases, the effect of AW tends to be more effective. However, note that the response becomes slow if b is too large. Despite some visual improvement, the performance is still sensitive to the change of AW gain. This sensitivity of AW gain needs to be considered carefully in the actual implementation of the control system.

Stability Analysis

The stability analysis of AWC is based on the nonlinear describing function analysis. Some previous studies made extensive investigation on the stability of AWC,[4] but we select the classical describing function approach, which provides direct physical insight over the AWC of this study. The linearized short-period pitch dynamics is given by a transfer function as

$$\frac{\theta(s)}{\delta_z(s)} = \frac{m_\delta s + (Z_\delta m_\alpha - Z_\alpha m_\delta)}{s^3 + (-Z_\alpha - m_q)s^2 - (m_\alpha - Z_\alpha m_q)s} \tag{6}$$

where $\delta_z(s)$ is elevator input, $\theta(s)$ is pitch attitude, and other parameters are aerodynamic stability derivatives. A detailed discussion on the describing function technique is well presented in Ref. 6. We go directly to the key features of the describing function approach. We observe that the describing function of a generic nonlinear element is expressed as[6]

$$K_N(X, \omega) = (Y_1/X)\angle\phi_1 \tag{7}$$

where X is the amplitude of the input sinusoid and Y_1 is the amplitude of the fundamental harmonic component of the output. The closed-loop characteristic equation with the nonlinear element replaced by its describing function becomes

$$1 + G_{eq}(jw)K_N(X, \omega) = 0 \tag{8}$$

where G_{eq} is the equivalent transfer function forming the closed-loop. The Nyquist diagram for $G_{eq}(j\omega)$ and $-1/K_N(X, \omega)$ are plotted in Fig. 2 for several values of b. Note that the larger value of b implies dominant AWC action over the integral control action. We start from a very small value of b and increase the value gradually by observing the resultant trends. It turns out the transfer function $G_{eq}(s)$ remains as a minimum-phase system for a certain range of b. If b exceeds a critical value the numerator polynomial comes to right half-plane zeros. The numerical data for the parameter b are set to be $b = [0.01, 0.1, 0.3, 0.4]$. In Fig. 2, case I corresponds to the smallest element of b, whereas case IV is matched with the largest element of b. Also the nonlinear describing function is plotted in the same complex plane. The describing function is a pure real number and plotted on the negative real axis. The slope of the saturation element is set to unity in the calculation of the describing function. Thus, the describing function trajectory starts from $(-1, 0)$ point. From Fig. 2 it is easy to understand that there is no limit cycle existent that is a crossing point between $G_{eq}(j\omega)$ and $-1/K_N(X, \omega)$. Even for the smallest element of b (case I), which is close to the case without AWC action, no limit cycle is observed. But the Nyquist diagram is observed to be parallel to the real axis for smaller b in the range of small ω. On the other hand, as the element of b increases, the Nyquist diagram moves farther from the critical point $(-1, 0)$. The diagram itself approaches the imaginary axis for small ω. Thus, heavier AWC action implies more stability in the sense of the describing function analysis.

Modified AWC

As already stated, too high a value of the AW gain may effectively reduce the amount of overshoot, but may also lead to a slow response. These phenomena are because the difference between the compensator output and the actuator control input with a high-AW gain gives a large-AW feedback signal in the initial control phase. The difference is primarily due to the proportional derivative (PD) terms of the compensator. This AW feedback signal drives the integrator to a large negative value. As time progresses, the PD terms of the compensator decrease, but the integrator output will not increase fast enough to compensate this change. This causes the compensator output to be small, eventually slowing down the control system responses. Although the proper selection of the AW gain may bring satisfactory response characteristics, some types of modeling errors are expected. These errors are also related to the sensitivity of the AW gain and the associated system responses. Therefore, it may be necessary to develop a controller structure less sensitive to changes

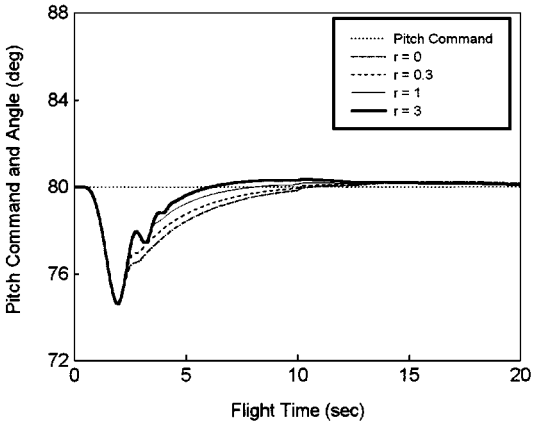

Fig. 3 Simulation results by modified AWC with $b = 1.0$.

in the control parameters. With this in mind, the preceding AWC is modified so that the modified AWC protects the integrator from being a large negative value in the initial control phase by limiting the PD terms of the compensator output for the AW feedback. In other words, if we let δ_{p1} and δ_{p2} represent the PD and integral terms of the compensator output, respectively, the controller takes the saturated values of δ_{p1} and δ_{p2} as the AW feedback signal. The modified AWC approach is constructed as

$$f = (1/T_t)\left[\min(\delta_{p1}, H) - u_p^w + \delta_{p2}\right] \tag{9}$$

where H is the saturated value of δ_{p1}, which limits the combination of proportional and derivative terms of the compensator output. A ratio of the saturated value of the actuator to H determines the modification quantities in the modified AWC

$$r = H_{\text{act}}/H \tag{10}$$

where H_{act} is the saturated values of the actuator, which is 22 deg for S-19. The attitude control performance of this modified AWC is presented in Fig. 3. It represents a case when the modified AWC is applied to the typical AWC with a large value of AW gain b. This case also corresponds to the slow response, as was discussed earlier. Note that the response characteristic has improved significantly. The change in the control system performance is not very large considering the same range of variation of r as in the AW gain of Fig. 1. These results prove the desirable performance of the modified AWC for the case of slow dynamic responses. It also shows that the modified AWC is not that sensitive to changes of the control parameter r. On the other hand, as the parameter r increases, the stability margin of the control system reduces gradually. However, closed-loop stability is guaranteed with the modified AWC if the original PID controller is stable.

Conclusions

Design of a typical and a modified AWC in the presence of actuator saturation of KSR-II is investigated. The control performance of the typical AWC turned out to be rather sensitive to the AW gain with slower response characteristics for a large AW gain. This has been partially resolved by introducing a modified AWC. The modified AWC improved the slow response considerably, even with a large AW gain. This modified AWC showed less sensitivity to the control gains compared with the typical AWC.

References

[1]Ljunge, L., and Hall, L., "S19 Guidance of the Black Brant X Sounding Rocket," *Journal of Guidance, Control, and Dynamics*, Vol. 7, No. 2, 1984, pp. 156–160.

[2]Hanus, R., Kinnaert, M., and Henrotte, J. L., "Conditioning Technique, a General Anti-Windup and Bumpless Transfer Method," *Automatica*, Vol. 23, No. 6, 1987, pp. 729–739.

[3]Kothare, M. V., Campo, P. J., Morari, M., and Nett, C. N., "A Unified Framework for the Study of Anti-Windup Designs," *Automatica*, Vol. 30, No. 12, 1994, pp. 1869–1883.

[4]Megretski, A., and Rantzer, A., "System Analysis via Integral Quadratic Constraints," *IEEE Transactions on Automatic Control*, Vol. 42, No. 6, 1997, pp. 819–830.

[5]Kothare, M. V., and Morari, M., "Multiplier Theory for Stability Analysis of Anti-Windup Control Systems," *Proceedings of the 34th Conference on Decision and Control* (New Orleans, LA), 1995, pp. 3767–3772.

[6]Nagraph, I. J., and Gopal, M., *Control Systems Engineering*, Wiley, New Delhi, India, 1982, pp. 625–642.

Artificial Lagrange Points for a Partially Reflecting Flat Solar Sail

Colin R. McInnes*
University of Glasgow, Glasgow, Scotland G12 8QQ, United Kingdom

I. Introduction

PREVIOUS studies have demonstrated that families of artificial Lagrange points may be generated using solar sail spacecraft.[1,2] However, these studies assumed an idealized solar sail with perfect reflectivity. This Note will reexamine the problem with a partially reflecting solar sail because a real aluminized sail film would typically have a reflectivity on the order of 0.9. First, equilibrium solutions will be obtained for an ideal flat solar sail. Then the problem will be revisited with a partially reflecting solar sail. Apart from reducing the magnitude of the radiation pressure force exerted on the solar sail, the finite absorption of the sail means that the radiation pressure force vector is no longer directed normal to the sail surface. Because of this effect, it will be shown that the volume of space available for artificial Lagrange points is extremely sensitive to the solar sail reflectivity. These artificial Lagrange points are of interest for a number of mission applications.[3–5]

II. Equilibrium Solutions for an Ideal Flat Solar Sail

First equilibrium solutions for an idealized, perfectly reflecting flat solar sail will be generated. We will not consider compound solar sails such as the solar photon thruster concept of Forward.[6] The ideal sail will be considered in a frame of reference corotating with two primary masses m_1 (Sun) and m_2 (Earth or another planet) at constant angular velocity $\boldsymbol{\omega}$, as shown in Fig. 1. The sail attitude is defined by a unit vector $\boldsymbol{n}$ normal to the sail surface, fixed in the rotating frame of reference. In addition, the ratio of the solar radiation pressure force to the solar gravitational force exerted on the sail is defined by the sail lightness number β. Because both forces have an inverse square variation with solar distance, the sail lightness number is a constant. It can be shown that the sail lightness number is related to the total solar sail mass per unit area by $\sigma\,(\mathrm{g\,m^{-2}}) = 1.53/\beta$. The units of the problem will be chosen such that the gravitational constant, the distance between the two primary masses, and the sum of the primary masses are all taken to be unity.

The vector equation of motion for a solar sail in this rotating frame of reference may be written in standard form as

$$\frac{\mathrm{d}^2\boldsymbol{r}}{\mathrm{d}t^2} + 2\boldsymbol{\omega} \times \frac{\mathrm{d}\boldsymbol{r}}{\mathrm{d}t} + \nabla U = \boldsymbol{a} \tag{1}$$

where the three-body gravitational potential U and the solar radiation pressure acceleration $\boldsymbol{a}$ are defined by

$$U = -\left\{\tfrac{1}{2}(x^2 + y^2) + [(1-\mu)/r_1] + (\mu/r_2)\right\} \tag{2a}$$

$$\boldsymbol{a} = \beta\left[(1-\mu)/r_1^2\right](\hat{\boldsymbol{r}}_1 \cdot \boldsymbol{n})^2\boldsymbol{n} \tag{2b}$$

Received June 12, 1998; revision received Aug. 17, 1998; accepted for publication Sept. 7, 1998.

*Reader, Department of Aerospace Engineering. E-mail: colinmc@aero.gla.ac.uk.